Journal of Oceanology and Limnology

https://doi.org/10.1007/s00343-026-5264-8

Research Paper

Multi-parameter evaluation of HYCOM forecasting performance in the South China Sea*

Mengli ZHANG, Jianping WU**, Jiagen LI**

College of Meteorology and Oceanography, National University of Defense Technology, Changsha 410073, China

Received Jul. 11, 2025; accepted in principle Feb. 28, 2026; accepted for publication Apr. 10, 2026

© Chinese Society for Oceanology and Limnology, Science Press and Springer-Verlag GmbH Germany, part of Springer Nature 2026

Abstract The Hybrid Coordinate Ocean Model (HYCOM) is an important tool for ocean research and forecasting. This study presents a comprehensive multi-parameter evaluation of HYCOM performance in the South China Sea (SCS) during 2019–2023, using multi-source satellite observations and reanalysis datasets. The modeled sea surface temperature (SST) closely matches satellite observations in its temporal evolution, although a systematic cold bias of approximately -0.1 °C remains, likely due to excessively strong vertical mixing. The model also fails to accurately reproduce the interannual declining trend of sea surface salinity (SSS), with a mean difference of 0.33 compared to Soil Moisture Active Passive (SMAP) observations, which is related to inaccuracies in the initial fields. The simulation of surface dynamical processes shows that modeled currents are stronger than observed in the northern SCS but weaker off southeastern Vietnam (around 10°N). One of the reasons for these current errors is the uncertainty in the Navy Global Environmental Model (NAVGEM) wind forcing used in HYCOM. While the upper ocean (0–1 000 m) shows relatively large temperature and salinity errors, with maximum root mean square error (RMSE) values of 0.88 °C and 0.39, the deep-water layer (>1 000 m) exhibits higher accuracy, with temperature RMSE approaching 0.1 °C and mean salinity RMSE around 0.03. These findings enhance our understanding of HYCOM's regional applicability and offer valuable guidance for the development of high-resolution ocean forecasting systems in the SCS.

Keyword: multi-parameter evaluation; Hybrid Coordinate Ocean Model (HYCOM); South China Sea; error mechanism analysis

1 INTRODUCTION

With the increase in computational capabilities, numerical ocean modeling and data assimilation techniques have significantly progressed, providing high-resolution global ocean products. The Global Ocean Forecasting System (GOFS), based on the HYCOM+Navy Coupled Ocean Data Assimilation (NCODA) framework, provides high-resolution global forecasts of ocean states and environmental variables. These outputs serve as valuable datasets for studying ocean dynamics. Previous studies have used HYCOM reanalysis data to investigate the variability of the deep SCS circulation (Zhu et al., 2022), the generation mechanism of the counter-wind SCS Warm Current (Yu et al., 2021), and the residual circulations and associated water mass transport in the SCS (Uchiyama et al., 2019). Trott et al. (2023) analyzed the amplitude, radius, and eddy kinetic energy of mesoscale eddies in the Luzon Strait based on HYCOM reanalysis, simulation, and forecast data. Zhai et al. (2014) used HYCOM assimilation data to investigate western boundary currents in the tropical northwestern Pacific, demonstrating that the mean velocity structure and standard deviations of the North Equatorial Current, Mindanao Current, and Kuroshio Current aligned with previous observations. The increase in the accuracy of these models requires more

* Supported by the National Key R&D Program of China (No. 2024YFC3109200), the National Natural Science Foundation of China (Nos. 42506030, 62372460), and the Innovation Research Foundation of National University of Defense Technology (No. ZK24-49)

** Corresponding authors: wjp@nudt.edu.cn; lijiagen@nudt.edu.cn

quantitative and rigorous comparisons with observations in order to understand how well they reproduce ocean dynamics and thermodynamics.

Previous studies have conducted evaluations and validations of HYCOM data, revealing its capability in depicting marine environmental elements. Kelly et al. (2007) compared the path and strength of the Kuroshio Extension (KE), along with the upper ocean heat budget, and found that the mean intensity and trajectory of the KE were consistent with satellite observations. Kara et al. (2008) conducted a multi-metric statistical evaluation of HYCOM SST against satellite and buoy data, reporting a median RMSE of 0.83 °C. Additionally, some studies compared the advantages and disadvantages of HYCOM and other products. Hyun et al. (2022) compared and verified the data of Nucleus for European Modelling of the Ocean (NEMO) and HYCOM using Argo profiles and drifting buoys. The results show that NEMO temperatures are more reliable than HYCOM. De Souza et al. (2021) conducted a comprehensive intercomparison of four global ocean reanalysis products (Global Ocean Physics Reanalysis (GLORYS), BlueLink Reanalysis (BRAN), HYCOM, and Climate Forecast System Reanalysis (CFSR)) in seas around New Zealand. The results showed that the GLORYS reanalysis performed better in general, and all four reanalysis products had large deviations in temperature and salinity, especially in coastal areas. Russo et al. (2022) noted that BRAN performed better in simulating mixed layer depth, while GLORYS and HYCOM exhibited warm biases. GLORYS more accurately represented Agulhas Current transport, while BRAN and HYCOM overestimated the southwest current. The comparative analysis reveals that HYCOM exhibits limited capability in accurately representing certain physical processes compared with other data products.

The SCS is a semi-enclosed deep-sea basin characterized by numerous islands, significant variations in water depth, and complex submarine topography. Ocean currents in this region are influenced by monsoons, bathymetry, and atmospheric circulation, exhibiting strong seasonal and spatial variability (Liu et al., 2001; Li et al., 2003). Additionally, deep-water circulation in the SCS is shaped by topography and thermohaline structures, forming a highly complex hydrodynamic system. Therefore, it is particularly important to conduct a systematic evaluation of HYCOM's performance in the SCS. Most comparisons of high-resolution models with observations have focused on comparisons of mean properties, analyses of the sea surface height (SSH) and SST variance, or on transport estimates at specific locations where the model may or may not perform well (Russo et al., 2022). Tracing the sources of model errors is critical for targeted improvements and enhanced forecast accuracy. Moreover, a systematic evaluation of HYCOM's performance in the SCS remains lacking. Therefore, we conduct a comprehensive evaluation of the HYCOM analysis data's capability in characterizing the marine environment of the SCS, based on satellite observations and reanalysis data. We further explore potential error mechanisms, providing insights for model improvement and enhancing HYCOM's practical applicability in the SCS.

2 DATA

2.1 HYCOM data

This study used output data from the GOFS 3.1 on the GLBy0.08 grid. GOFS 3.1, based on the HYCOM and NCODA system, provides global ocean state forecasts. Variables such as temperature, salinity, current, and SSH from 2019 to 2023 were selected to evaluate the dataset's characterization capability in the SCS. The dataset has a spatial resolution of 1/12°, a temporal resolution of 3 h, and 40 vertical layers.

2.2 Observation

The satellite-observed SST data were obtained from the Optimum Interpolation Sea Surface Temperature (OISST) product provided by the National Oceanic and Atmospheric Administration. This product integrates observations from multiple platforms (satellites, ships, buoys, and Argo floats) into a regular global grid with a spatial resolution of 0.25°×0.25° and daily temporal resolution.

The SMAP SSS V6.0 validated data were obtained from Remote Sensing Systems. The product includes three data types: Level 2C swath data, Level 3 8-d running averages, and Level 3 monthly averages. This study used the Level 3 monthly product with a spatial resolution of 0.125°×0.125°.

The SSH and current data were obtained from the Copernicus Marine Service center (product ID is SEALEVEL_GLO_PHY_L4_MY_008_057). This product provides additional variables, such as Absolute Dynamic Topography (ADT) and geostrophic currents, with daily and monthly temporal resolutions, a spatial resolution of 0.25°×

0.25°, and coverage from January 1993 to May 2025.

The World Ocean Atlas (WOA) is a collection of objectively analyzed, quality-controlled temperature, salinity, oxygen, phosphate, silicate, and nitrate means based on profile data from the World Ocean Database. This study selects WOA 2023, which has a spatial resolution of 0.25°×0.25° and is vertically divided into 102 layers (0–5 500 m).

2.3 Analysis and reanalysis

HYCOM is forced by the NAVGEM atmospheric forecast system, which was developed by the U. S. Naval Research Laboratory. The NAVGEM products have a temporal resolution of 3 h and a spatial resolution of 0.175 8°.

The net radiation (longwave and shortwave) and turbulent (latent and sensible) heat fluxes used in the evaluation of HYCOM are all sourced from the European Centre for Medium-Range Weather Forecasts Reanalysis v5 (ERA5) reanalysis dataset. The NAVGEM wind field is assessed using the ERA5 and Cross-Calibrated Multi-Platform (CCMP) products as references.

3 RESULT

3.1 Sea surface temperature

The comparison between the modeled SST and satellite observations shows a highly consistent spatial distribution of standard deviations from 2019 to 2023 (Fig.1a & b). Compared to the southern SCS, SST variations are more pronounced in the northern region, especially in the Taiwan Strait, along the Guangdong coast, and the Beibu Gulf. Moreover, the mean SST difference (Fig.1c) is relatively larger in these regions. HYCOM exhibits a cold bias within 0.5 °C in most parts of the SCS, with an average difference of -0.1 °C. The SST difference is more pronounced near the Guangdong coast and the Taiwan Strait. Figure 1e shows the temporal variation of SST anomalies (SST-WOA 23) of the model and satellite observations, revealing a strong correlation (R=0.996 5). However, differences still exist in the long-term fluctuation between the modeled SST and satellite observations, especially during summer and winter. The spatial distribution of SST RMSE and its temporal trend are shown in Fig.1d & f, respectively. The SST RMSE is larger in coastal regions (the maximum is 0.5 °C). During 2019–2023, the SST RMSE is less than 0.45 °C, larger in winter and smaller in summer.

Given that SST variations are primarily driven by surface heat fluxes on seasonal timescales (Vivier et al., 2002; Kelly and Dong, 2004), this study compared the net surface heat flux from HYCOM (model output) with that from ERA5. In regions such as the Beibu Gulf, along the Guangdong coast, and in the central SCS (the Taiwan Strait and the southern basin), the HYCOM net heat flux is greater (smaller) than ERA5 (Fig.2a), while the modeled SST in those same areas is lower (higher) than satellite observations (Fig.1c). Furthermore, the

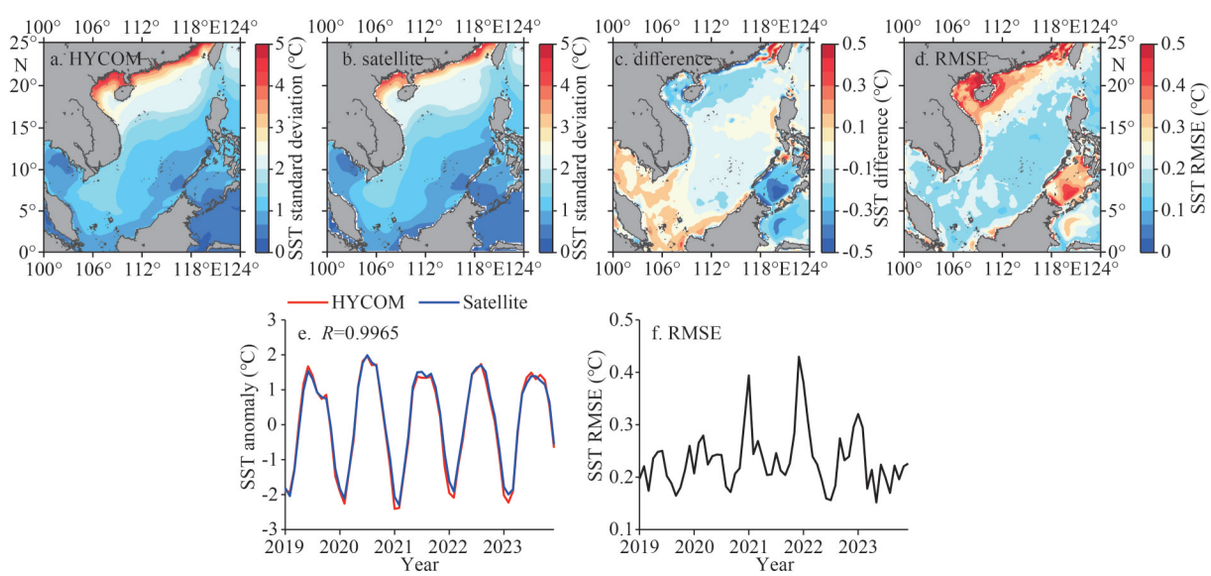


Fig.1 Comparisons of observed and modeled sea surface temperature (SST)

a–b. spatial distribution of SST standard deviation; c. spatial distribution of time-averaged SST difference (HYCOM-satellite observations); d. spatial distribution of SST root mean square error (RMSE); e–f. temporal variation of spatially averaged SST anomalies (e) and RMSE (f).

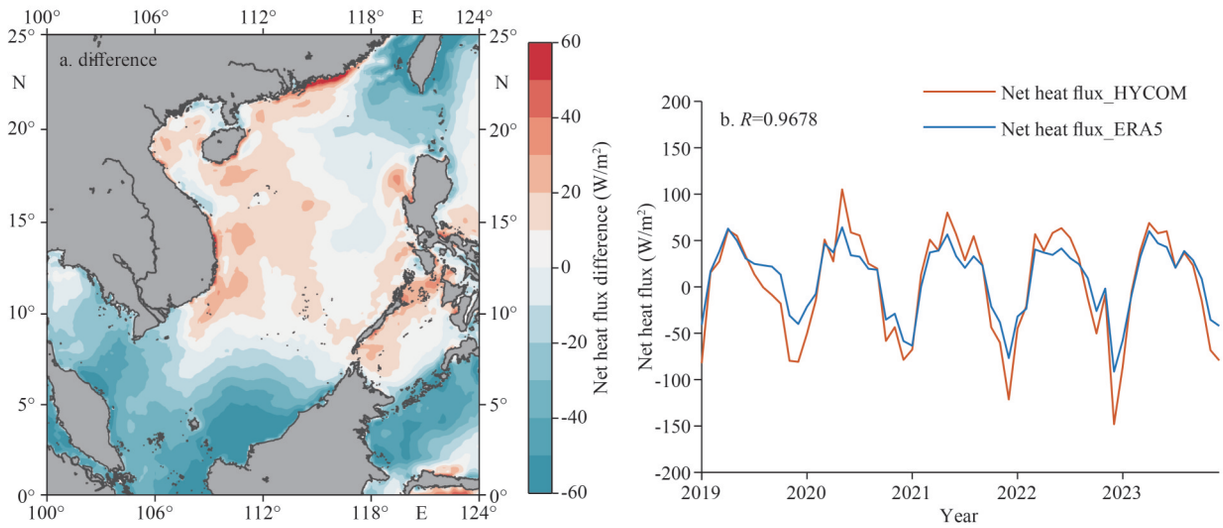


Fig.2 Time-averaged difference of net surface heat flux (HYCOM-ERA5) (a), temporal variations of spatially averaged net surface heat flux (b)

HYCOM net heat flux is smaller than ERA5 during winter (Fig.2b), which corresponds well with the observed lower SST in HYCOM during winter (Fig.1e). However, in the summers between 2020 and 2022, the HYCOM net heat flux is greater than ERA5, yet the SST remains underestimated during the same periods. Therefore, surface net heat flux is likely not the primary factor causing the SST cold bias in the model. Some of the flux differences are owing to the use of different ERA products (Kelly et al., 2007) or to issues in the surface flux parameterization schemes of HYCOM.

This study conducted a mixed layer heat budget analysis (Qu, 2003) to further reveal the factors responsible for the SST cold bias.

$$\frac{\partial T_{\mathrm{m}}}{\partial t}=\frac{Q_{\mathrm{net}}-q(-h_{\mathrm{m}})}{\rho_0 c_p h_{\mathrm{m}}}-U\cdot\nabla T_{\mathrm{m}}-\frac{w_{\mathrm{ent}}\Delta T}{h_{\mathrm{m}}}+R, \quad (1)$$

where, T_{m} is the mixed layer temperature; Q_{net} is the net surface heat flux; h_{m} is the mixed layer depth; ρ_0 is the seawater density, taken as 1 027 kg/m^3; c_p is the specific heat capacity of seawater, taken as 4 000 J/(kg·°C); the horizontal velocity U includes both the geostrophic ($\boldsymbol{u}_g$) and Ekman ($\boldsymbol{u}_e$) components; ΔT is the temperature difference between the mixed layer and just below the mixed layer; w_{ent} is the entrainment rate, following Qu (2003), w_{ent} can be determined by

$$\begin{cases} w_{\mathrm{ent}}=\dfrac{\partial h_{\mathrm{m}}}{\partial t}+w_{\mathrm{mb}}+\vec{U}\cdot\nabla h_{\mathrm{m}}, \\ \text{if } \dfrac{\partial h_{\mathrm{m}}}{\partial t}+w_{\mathrm{mb}}+\vec{U}\cdot\nabla h_{\mathrm{m}}>0, \\ w_{\mathrm{ent}}=0, \text{ otherwise}, \end{cases} \quad (2)$$

where, w_{mb} is the velocity of water parcel at the base of the mixed layer. $q(-h_{\mathrm{m}})$ is the downward radiative heat flux at the bottom of the mixed layer (Paulson and Simpson, 1977):

$$q(-h_{\mathrm{m}})=q(0)\left[R\mathrm{e}^{\left(\frac{-h_{\mathrm{m}}}{\gamma_1}\right)}+(1-R)\mathrm{e}^{\left(\frac{-h_{\mathrm{m}}}{\gamma_2}\right)}\right], \quad (3)$$

where, $q(0)$ is the downward shortwave radiative flux at the sea surface. The attunation coefficients are selected for a Type IA water (Jerlov, 1968), R= 0.62, γ_1=0.6 m, and γ_2=20 m. The left side of the Eq.1 is temperature trend. On the right side, the first term is the heat flux, the second term is the horizontal advection (Adv), the third term is the vertical entrainment (ENT), and the last term is the residual (R).

Figure 3 shows the variations of the heat budget terms and their absolute contribution rates. On the interannual timescales, both the net heat flux and entrainment term exert significant influences on temperature variability, with absolute contribution rates of 35.84% and 28.14%, respectively. These two terms account for 64% of the total contribution, essentially determining the variability of mixed-layer temperature. In contrast, the contributions from advection and q term are relatively small (15.72% and 10.97%). On the interannual timescales, the net heat flux and entrainment contribute significantly to the mixed layer heat budget of the SCS, whereas advection plays an important role mainly in the ocean below the mixed layer (Taguchi et al., 2017; Song et al., 2019).

This study further analyzes the spatial distribution of the heat budget terms (Fig.4a–c). The

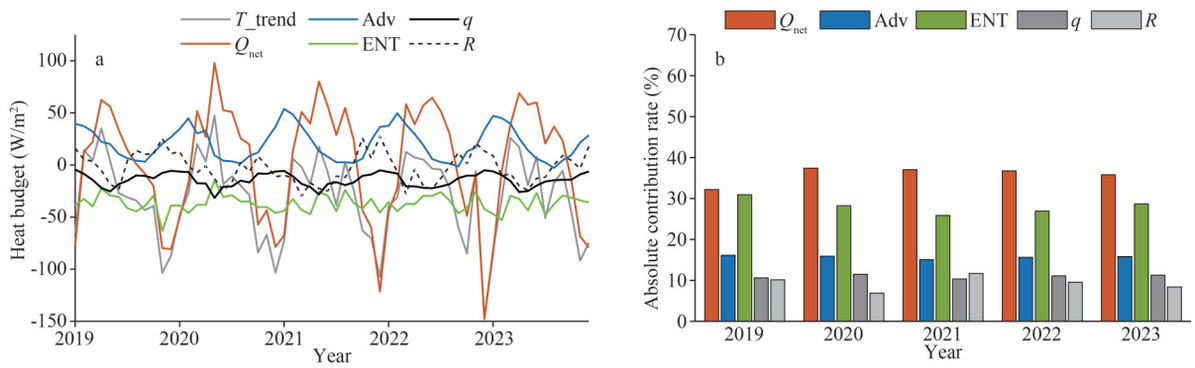


Fig.3 Domain-averaged heat budget (a) and their absolute contributions (b)

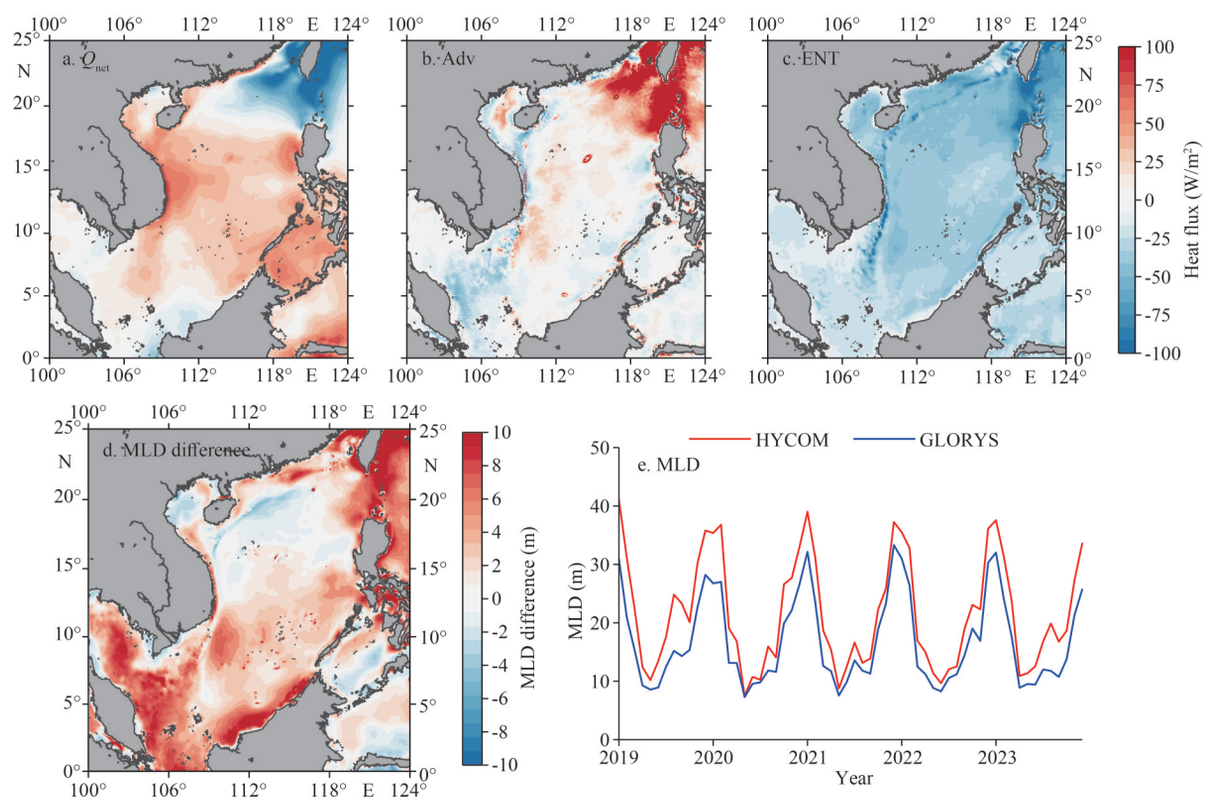


Fig.4 The spatial distribution of the net heat flux term (a), the horizontal advection term (b), the vertical entrainment term (c), the mixed layer depth (MLD) differences (d, HYCOM-GLORYS), and the temporal variation of MLD (e)

results show that the advection term generally exhibits an opposite sign to the net heat flux term, indicating the important role of ocean circulation in balancing the heat flux forcing in the heat budget. However, the net heat flux is not the dominant factor responsible for the SST cold bias, and the contribution of advection to mixed-layer temperature variability is also relatively small. Therefore, this study focuses on the role of the entrainment term. Vertical entrainment represents a cooling effect by entraining cold water from below into the mixed layer. In regions with pronounced SST cold biases, such as the northern SCS and the Beibu Gulf, the cooling induced by entrainment is also more evident (Figs.1c & 4c). In addition, compared with the GLORYS reanalysis, the mixed layer depth (MLD) simulated by HYCOM is generally deeper over the SCS (Fig.4d–e). This difference may imply stronger vertical mixing in HYCOM, leading to enhanced upwelling of colder water and consequently contributing to the SST cold bias in the model.

3.2 Sea surface height and current

In this study, the ADT field is used to validate the

modeled SSH. Since the reference planes of ADT and modeled SSH are different, the time average of each field is subtracted separately to obtain comparable anomaly fields, which are uniformly referred to as sea surface height anomaly (SSHA). SSHA variations are strong along the Guangdong coast, the Vietnam coast, the waters west of Luzon Island, and the Gulf of Thailand (Fig.5a & b). The average SSHA difference in the SCS is approximately -0.02 cm. In the northern SCS, the modeled SSHA is greater than the satellite observations (indicated as a positive difference in Fig.5c), while in the central and southern regions, the modeled SSHA is generally lower than the satellite observations (indicated as a negative difference in Fig.5c). The RMSE of SSHA is less than 4 cm in most parts of the SCS, with relatively larger RMSE values only in the waters west of Luzon Island and the Gulf of Thailand. The time series comparison of SSHA between the model and satellite observations (Fig.5e) reveals distinct differences in their long-term variability. As indicated by the red and blue lines in Fig.5e, the modeled SSH was greater than the satellite observation from January 2019 to May 2021, then became smaller, and became larger again after May 2023.

Figure 6 illustrates the seasonal variations of the modeled sea surface current and velocity compared to satellite observations. In autumn and winter, compared with satellite observations, the cyclonic circulation in the northern SCS simulated by HYCOM was stronger. North of 17°N, the average current velocity of HYCOM and satellite observation was about 0.17 and 0.13 m/s, respectively. In addition, in terms of the Kuroshio's intrusion into the SCS, the model results are stronger than the satellite observations (by approximately 30.8%). In spring and summer, the modeled current is basically consistent with the satellite observations. In the Vietnam Coastal Current (around 10°N), the modeled current is weaker than the satellite observations in all four seasons. Wind stress plays a crucial role in the seasonal variations of circulation in the SCS (Yang and Liu, 1998; Qu, 2000). Errors in the simulated current and SSH may stem from insufficient accuracy in the wind forcing used in HYCOM.

The SCS is dominated by northeasterly winds in winter and southwesterly winds in summer, with the winter monsoon being significantly stronger than the summer monsoon. As shown in Fig.7, off southeastern Vietnam (around 10°N), NAVGEM wind stress shows slightly weaker than ERA5 and CCMP during summer, which corresponds to the weaker modeled current for the same region (Fig.6a2 & a4). In the northern SCS, NAVGEM wind stress exhibits higher than ERA5 and CCMP during autumn and winter (particularly noticeable in

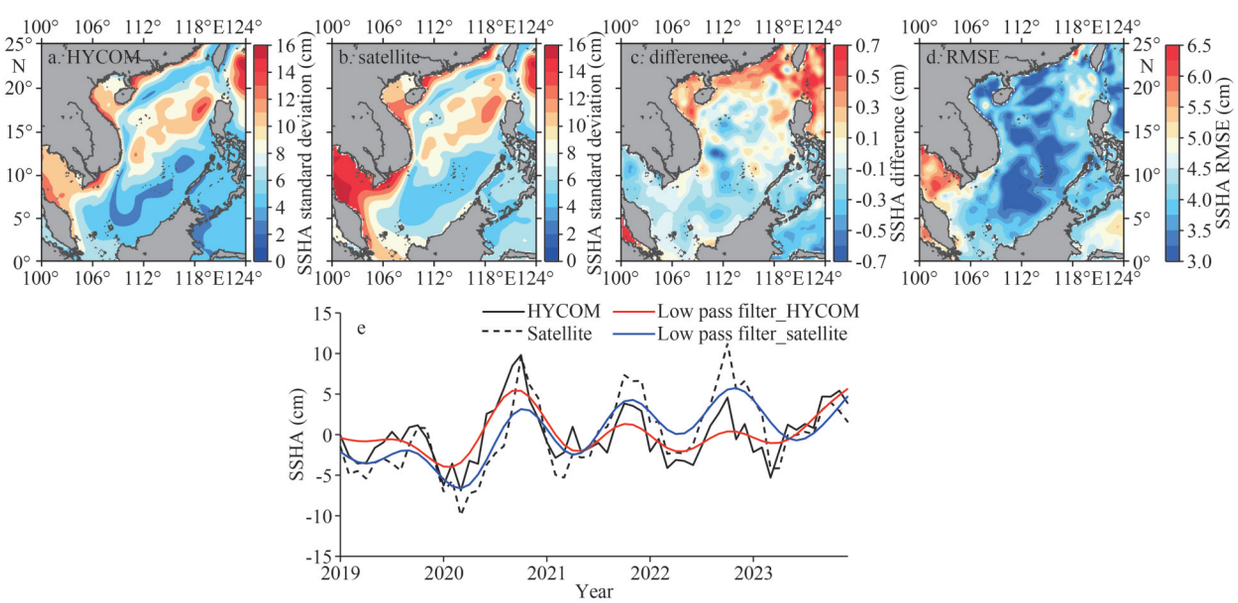


Fig.5 Spatial distribution of sea surface height anomaly (SSHA) standard deviation (a–b), time-averaged difference (c), and root mean square error (RMSE) (d); temporal variation of spatially averaged SSHA (e)

The solid and dashed lines in (e) are SSHA from the HYCOM and from altimeter respectively, while the red and blue heavy lines in (e) are the corresponding low-pass-filtered SSHA.

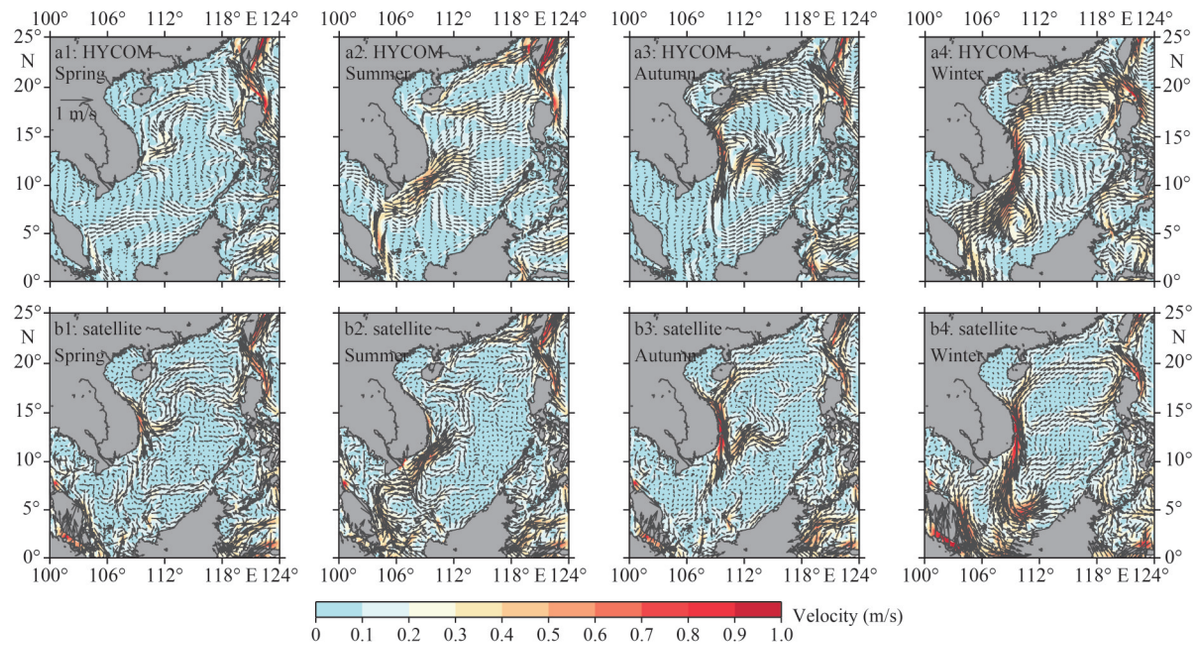


Fig.6 Seasonal variations of current and velocity in HYCOM (a1–a4) and satellite observations (b1–b4)

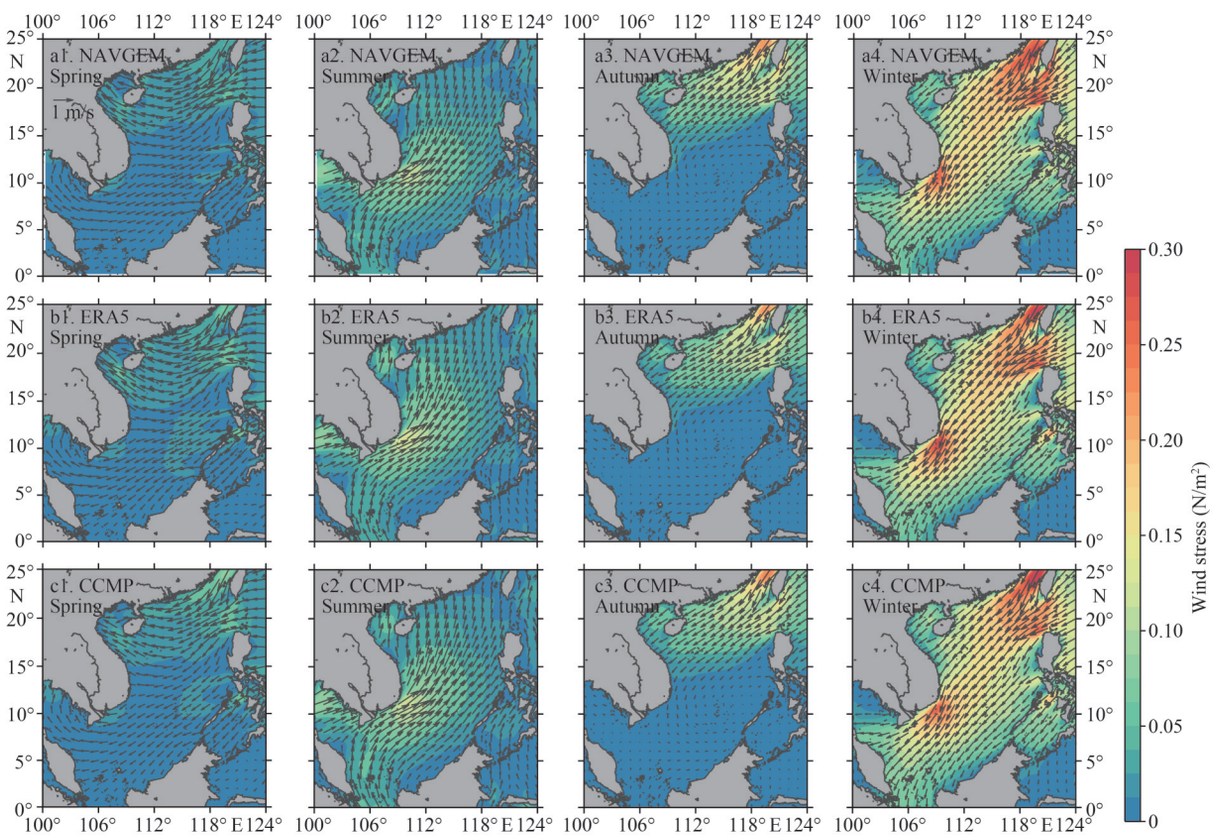


Fig.7 Seasonal variations of wind stress in NAVGEM (a1–a4), ERA5 (b1–b4), and CCMP (c1–c4)

The grey arrow is the 10-m wind vector.

the Taiwan Strait and Luzon Strait), leading to stronger coastal currents off Guangdong and intensified cyclonic circulation in the northern SCS (Fig.6a3 & a4).

3.3 Sea surface salinity

The SMAP satellite-observed SSS data were used to validate the HYCOM data. Figure 8 shows the spatial distribution of the standard deviation, difference, and RMSE for both datasets. The high standard deviation values appear at the Zhujiang (Pearl) River estuary and along the Vietnam coast, where SSS varies greatly, while in most of the SCS, the standard deviation of SSS is below 0.5 (Fig.8a & b). It is noteworthy that the SSS variation amplitude observed by SMAP is greater than the model's, with an average difference of about 0.22. The SSS difference and RMSE maps both show that errors are generally larger in the coastal regions (Fig.8c & d).

This study further applies empirical orthogonal function (EOF) decomposition to the SSS from HYCOM and SMAP, with the results shown in Fig.9. The first mode explaining 57.18% and 64.23% of the variance, respectively. West of Luzon Island, the SMAP observations show a larger gradient of SSS variation, which is not reflected in HYCOM (Fig.9a & b). The time series of modeled SSS differs significantly from the satellite observations, particularly from 2020 to 2023 (Fig.9c). This suggests that HYCOM may not have captured the variations in SSS in the SCS well during 2019–2023.

Figure 10a shows the trend of SSS anomalies (SSS-WOA 23) for HYCOM, SMAP observations, and Simple Ocean Data Assimilation (SODA) during 2019–2023. The SSS anomalies of SMAP and SODA decrease year by year during this five-year period, with minimum values of -0.89 and -0.78, and the trend is basically the same (R=0.92). However, the modeled SSS anomalies fluctuate within ±0.3 during 2019–2023, with very weak interannual variations.

The SSS variations in the SCS are influenced by the El Niño-Southern Oscillation (ENSO) signal through two main mechanisms: (1) the "atmospheric bridge" formed by the Walker circulation (Zhang et al., 2019), which controls precipitation changes. During El Niño years, precipitation decreases, leading to an increase in SSS, while the opposite occurs during La Niña years (Guo, 2012; Wang and Huang, 2016); (2) ENSO influences the Kuroshio intrusion into the SCS. This study analyzed the trend of the Niño3.4 index (smoothed with a 3-month moving average), where values less than 0.5 were marked as La Niña events and values greater than

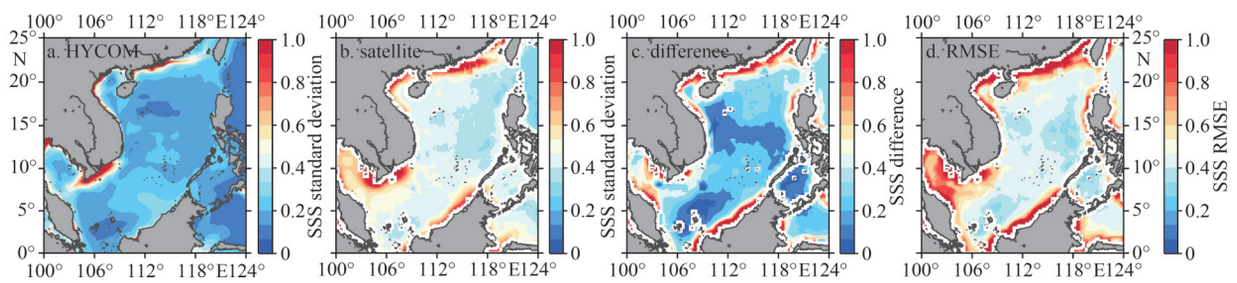


Fig.8 Comparisons of observed and modeled sea surface salinity (SSS)

a–b. spatial distribution of SSS standard deviation; c. spatial distribution of time-averaged SSS difference (HYCOM minus satellite observations); d. spatial distribution of SSS root mean square error (RMSE).

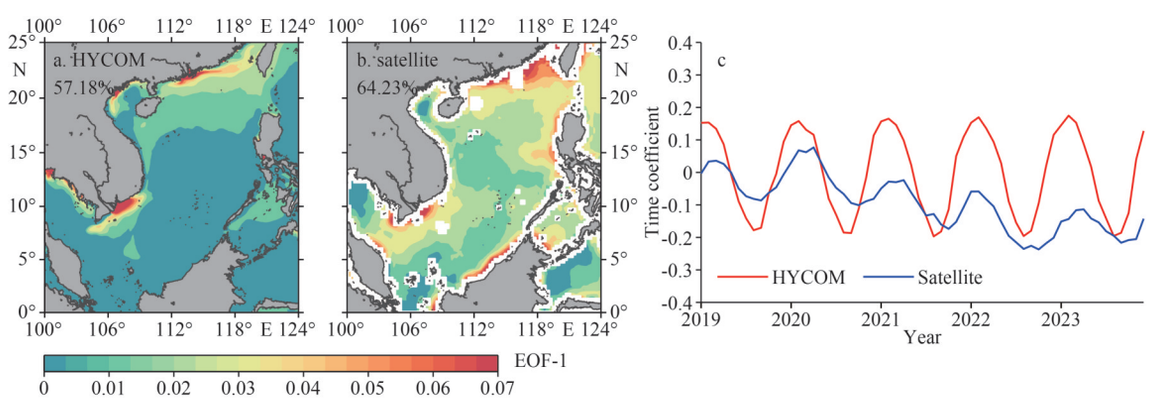


Fig.9 First mode spatial distribution (a–b) and time coefficient (c) of sea surface salinity (SSS) anomaly empirical orthogonal function (EOF) analysis for HYCOM and SMAP observations

0.5 as El Niño events. A continuous La Niña event occurred between June 2020 and February 2023 (Fig.10a), meaning that during this period, the SSS in the SCS should theoretically decrease. Both SMAP and SODA show a significant decreasing trend in SSS during the five years (approximately -0.23/a and -0.13/a, respectively), which aligns with the increase in freshwater flux caused by the persistent La Niña event. However, HYCOM fails to capture this trend.

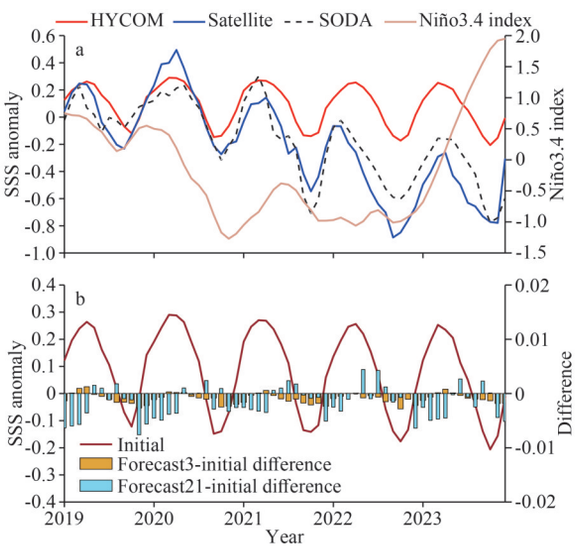


Fig.10 Spatially averaged sea surface salinity (SSS) anomalies comparison

a. comparison of SSS anomalies from HYCOM, SMAP, and SODA. The red and blue lines are the temporal variation trends of SSS anomalies from HYCOM and SMAP, respectively. The black dashed line is the SODA's 5-m layer salinity anomaly, and the pink line is the Niño3.4 index (3-month moving average); b. comparison of HYCOM SSS initial fields and forecast fields. The deep red line is the monthly averaged HYCOM SSS initial field (at 12:00:00). The orange (blue) bars are the difference between the 3-h (21-h) forecast field and the initial field.

To determine whether the differences between satellite observations and HYCOM originated from its SSS initial fields (daily at 12:00:00) or forecast fields, we conducted a comparative analysis of monthly-averaged SSS anomaly fields from 2019 to 2023, as well as their differences relative to 3-h and 21-h forecast fields (Fig.10b). It can be seen that the initial field's trend is almost identical to the red line in Fig.10a (average of all times for each month). Additionally, whether for the 3- or 21-h forecast fields, the difference between them and the initial field is very small, fluctuating within ±0.01. Therefore, the significant difference between the HYCOM SSS initial field and satellite observations during 2019–2023, resulting in a low simulation accuracy of SSS in the SCS. Even short-term forecasts are unable to correct the biases introduced by the initial conditions.

3.4 Vertical structure of temperature and salinity

Figure 11 displays the standard deviations and RMSE of the vertical temperature and salinity structures between HYCOM and WOA 2023. The standard deviations for temperature and salinity in both datasets are less than 1.55 °C and 0.20, respectively. From the surface to 1 000 m, the standard deviations of HYCOM temperature and salinity are generally larger than WOA, while below 1 000 m, the standard deviation approaches zero, indicating very small variations in temperature and salinity (Fig.11a). Figure 11c & d show the variation of temperature and salinity RMSE with depth. Both RMSE values are relatively high above 1 000 m, with maximum values of 0.88 °C and 0.39, respectively. In the depth range of 1 000–5 000 m, the temperature RMSE remains below 0.2 °C and gradually decreases toward 0.1 °C, while the salinity

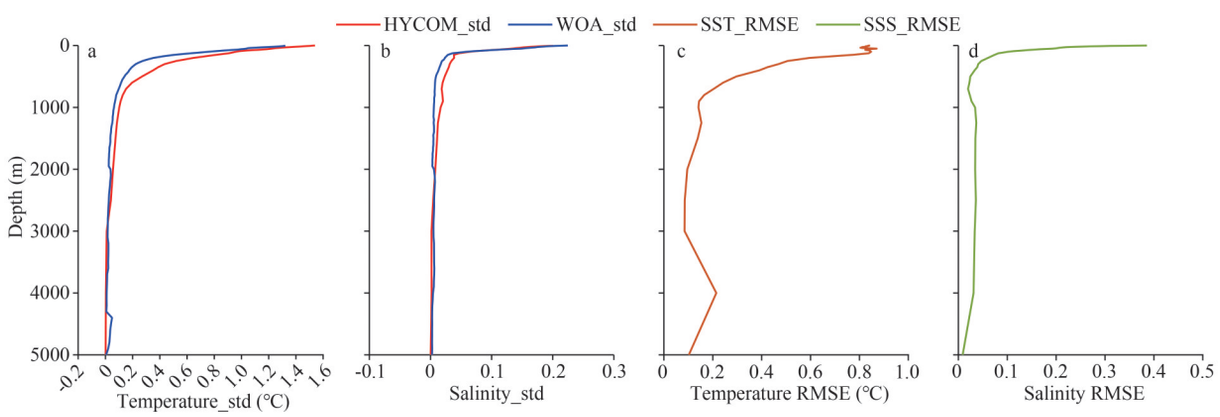


Fig.11 Standard deviation (a–b) and root mean square error (RMSE) (c–d) of the vertical temperature and salinity structures from HYCOM and WOA 2023

RMSE averages approximately 0.03. These results demonstrate that HYCOM's vertical salinity structure is nearly identical to WOA's. HYCOM demonstrates exceptional performance in simulating deep waters (>1 000 m), which can be attributed to its hybrid vertical coordinate scheme that effectively reproduces the deep circulation in the SCS (Wang, 2012).

4 DISCUSSION

HYCOM represents a substantial improvement over low-resolution models in reproducing characteristics of the SCS. However, differences still exist between the model results and satellite observations. We found that HYCOM exhibits SST cold bias over the SCS, particularly along the Guangdong coast and in the Beibu Gulf. The presence of this cold bias indicates a systematic error in the model's simulation of thermodynamic processes. Previous studies have shown that in the Asian-northwest Pacific monsoon region, the inconsistency between the surface heat flux provided by atmospheric models and that required by ocean models is one of the important causes of the SST cold bias in this region (Ren and Qian, 2005; Fang et al., 2010). However, this study indicates that net heat flux is not the primary factor contributing to the SST cold bias. Turbulent vertical mixing plays an important role in regulating SST, upper-ocean structure, and mixed-layer depth (Moum et al., 2013; Hummels et al., 2014, 2020). Through mixed-layer heat budget analysis, we find that regions with pronounced SST cold biases also exhibit stronger entrainment, and the modeled MLD is generally deeper compared to the GLORYS reanalysis. These results suggest that overly strong vertical mixing in HYCOM is likely an important contributor to the SST cold bias.

Errors in simulated surface currents primarily originate from uncertainties in external wind forcing, but are also influenced by internal physical processes represented in the model. For example, wave-induced mixing can modify upper-ocean stratification and energy distribution, thereby affecting circulation and climate variability (Qiao et al., 2006, 2010; Jing et al., 2025). Similarly, tidal mixing has been shown to enhance transport through the Luzon Strait, strengthen basin-scale cyclonic circulation, and intensify the meridional overturning circulation (Wang et al., 2017). In addition, inadequate representation of bathymetry may introduce pressure gradient errors and numerical noise, leading to spurious velocities and vorticity (Haney, 1991; Beckmann and Haidvogel, 1993). Given the highly complex topography of the SCS, accurate bathymetric representation is essential for realistically simulating deep circulation patterns (Wang, 2012) and the separation of the Vietnam coastal current (Gan and Qu, 2008). The quality of initial conditions also plays an important role in model performance (Hackert et al., 2007; Zheng and Zhu, 2015). In this study, the initial SSS field exhibited a mean bias of approximately 0.33 compared with SMAP observations during 2019–2023, which contributed to the model's inability to reproduce the observed interannual declining trend of SSS in the SCS. It is worth noting that, due to the lack of deep in-situ observations in the SCS during the simulation period, validation of deep currents remains limited and requires further observational support in future studies.

In addition, the evaluation period of this study was influenced by persistent La Niña events, during which regional precipitation, runoff, and upper-ocean structure deviated from the multi-year mean state. Consequently, the conclusions to some extent reflect the performance of HYCOM under anomalous climate conditions rather than its long-term "normal" performance.

5 CONCLUSION

This study analyzes and evaluates multiple oceanic environmental variables simulated by HYCOM in the SCS and explores the mechanisms responsible for simulation errors based on satellite observations and reanalysis data from 2019 to 2023. HYCOM SST exhibits a general cold bias in the SCS, which is particularly pronounced in the northern SCS, with a maximum difference of -0.5 °C. One possible cause of this cold bias is the overly strong vertical mixing in HYCOM, as indicated by its simulated MLD being significantly greater than that of the GLORYS reanalysis data. In terms of long-term temporal trends, HYCOM and satellite-observed SST show a significant correlation (R=0.996 5). However, HYCOM failed to accurately reproduce the interannual decreasing trend of SSS from 2019 to 2023, showing a mean bias of 0.33 compared to SMAP observations. This indicates that HYCOM has poor simulation performance for SSS in the SCS over this period, a conclusion further supported by comparisons with SODA and the Niño3.4 index. Additionally, we found that the large SSS errors in

HYCOM simulations may be attributed to the low accuracy of the initial fields used.

In the simulation of surface dynamical processes, the SSHA RMSE is less than 4 cm in most regions of the SCS. Compared to satellite observations (ERA5 and CCMP), the modeled surface currents (the NAVGEM wind stress) in the northern SCS are stronger during autumn and winter. In contrast, in the southeastern region off Vietnam (around 10°N), the modeled currents (the NAVGEM wind stress) are weaker during summer. One of the reasons for these current errors is the uncertainty in the NAVGEM wind forcing used in HYCOM. Evaluation of the vertical temperature and salinity structure shows that HYCOM exhibits large variability and high RMSEs in the upper 1 000 m, with maximum RMSE of 0.88 °C for temperature and 0.39 for salinity. Below 1 000 m, variability and RMSEs are minimal, with temperature RMSE around 0.1 °C and salinity RMSE around 0.03, indicating good performance in simulating deep-water characteristics.

This study evaluates the performance of HYCOM in simulating oceanic environmental variables in the SCS during 2019–2023. Although the evaluation period represents a relatively short timescale and coincided with anomalous climatic conditions, the results provide useful insights into the model's strengths and deficiencies in reproducing surface and subsurface variability. Model errors may be associated with uncertainties in atmospheric forcing, the quality of initial conditions, and limitations in physical parameterizations. Future efforts should focus on improving forcing and initial conditions accuracy, and refining physical schemes, especially those related to submesoscale and wave-induced mixing, to alleviate issues such as excessively deep MLD and enhance the overall reliability of HYCOM simulations in the SCS.

6 DATA AVAILABILITY STATEMENT

The datasets generated during or analyzed during the current study are available from the corresponding author on reasonable request.

References

Beckmann A, Haidvogel D B. 1993. Numerical simulation of flow around a tall isolated seamount. part I: problem formulation and model accuracy. *Journal of Physical Oceanography*, **23**(8): 1736-1753, https://doi.org/10.1175/1520-0485(1993)023<1736:NSOFAA>2.0.CO;2.

De Souza J M A C, Couto P, Soutelino R et al. 2021. Evaluation of four global ocean reanalysis products for New Zealand waters—a guide for regional ocean modelling. *New Zealand Journal of Marine and Freshwater Research*, **55**(1): 132-155, https://doi.org/10.1080/00288330.2020.1713179.

Fang Y J, Zhang Y C, Tang J P et al. 2010. A regional air-sea coupled model and its application over East Asia in the summer of 2000. *Advances in Atmospheric Sciences*, **27**(3): 583-593, https://doi.org/10.1007/s00376-009-8203-7.

Gan J P, Qu T D. 2008. Coastal jet separation and associated flow variability in the southwest South China Sea. *Deep Sea Research Part I*: *Oceanographic Research Papers*, **55**(1): 1-19, https://doi.org/10.1016/j.dsr.2007.09.008.

Guo J. 2012. Analysis of characters and mechanisms of the mixed layer salinity variation in South China Sea. First Institute of Oceanography, Ministry of Natural Resources, Qingdao, China. (in Chinese with English abstract)

Hackert E, Ballabrera-Poy J, Busalacchi A J et al. 2007. Comparison between 1997 and 2002 El Niño events: Role of initial state versus forcing. *Journal of Geophysical Research*: *Oceans*, **112**(C1): C01005, https://doi.org/10.1029/2006JC003724.

Haney R L. 1991. On the pressure gradient force over steep topography in sigma coordinate ocean models. *Journal of Physical Oceanography*, **21**(4): 610-619, https://doi.org/10.1175/1520-0485(1991)021<0610:OTPGFO>2.0.CO;2.

Hummels R, Dengler M, Brandt P et al. 2014. Diapycnal heat flux and mixed layer heat budget within the Atlantic Cold Tongue. *Climate Dynamics*, **43**(11): 3179-3199, https://doi.org/10.1007/s00382-014-2339-6.

Hummels R, Dengler M, Rath W et al. 2020. Surface cooling caused by rare but intense near-inertial wave induced mixing in the tropical Atlantic. *Nature Communications*, **11**(1): 3829, https://doi.org/10.1038/s41467-020-17601-x.

Hyun S H, Hwang S O, Lee S M et al. 2022. Verification of the KMA ocean model NEMO against Argo floats and drift buoys: a comparison with the up-to-date US navy HYCOM. *Atmosphere*, **32**(1): 71-84, https://doi.org/10.14191/Atmos.2022.32.1.071.

Jerlov N G. 1968. Optical Oceanography. Elsevier, London, p.199.

Jing Y J, Sun J, Li R et al. 2025. The impact of wave-induced mixing on the simulation of the upper mixed layer in climate models. *Ocean Modelling*, **197**: 102583, https://doi.org/10.1016/j.ocemod.2025.102583.

Kara A B, Metzger E J, Hurlburt H E et al. 2008. Multistatistics metric evaluation of ocean general circulation model sea surface temperature: application to 0.08° Pacific Hybrid Coordinate Ocean Model simulations. *Journal of Geophysical Research*: *Oceans*, **113**(C12): C12018, https://doi.org/10.1029/2008JC004878.

Kelly K A, Dong S. 2004. The relationship of western boundary current heat transport and storage to midlatitude ocean-atmosphere interaction. *In*: Wang C, Xie S P, Carton J A eds. Earth's Climate: The Ocean-

Atmosphere Interaction. Washington: American Geophysical Union, **147**: 347-363, https://doi.org/10.1029/147GM19.

Kelly K A, Thompson L, Cheng W et al. 2007. Evaluation of HYCOM in the Kuroshio Extension region using new metrics. *Journal of Geophysical Research*: *Oceans*, **112**(C1): C01004, https://doi.org/10.1029/2006JC003614.

Li L, Xu J D, Jing C S et al. 2003. Annual variation of sea surface height, dynamic topography and circulation in the South China Sea: a TOPEX/Poseidon satellite altimetry study. *Science in China Series D*: *Earth Sciences*, **46**(2): 127-138, https://doi.org/10.1360/03yd9012.

Liu Z Y, Yang H J, Liu Q Y. 2001. Regional dynamics of seasonal variability in the South China Sea. *Journal of Physical Oceanography*, **31**(1): 272-284, https://doi.org/10.1175/1520-0485(2001)031<0272:RDOSVI>2.0.CO;2.

Moum J N, Perlin A, Nash J D et al. 2013. Seasonal sea surface cooling in the equatorial Pacific cold tongue controlled by ocean mixing. *Nature*, **500**(7460): 64-67, https://doi.org/10.1038/nature12363.

Paulson C A, Simpson J J. 1977. Irradiance measurements in the upper ocean. *Journal of Physical Oceanography*, **7**(6): 952-956, https://doi.org/10.1175/1520-0485(1977)007<0952:IMITUO>2.0.CO;2.

Qiao F L, Ma J, Xia C S et al. 2006. Influences of the surface wave-induced mixing and tidal mixing on the vertical temperature structure of the Yellow and East China Seas in summer. *Progress in Natural Science*, **16**(7): 739-746, https://doi.org/10.1080/10020070612330062.

Qiao F L, Yuan Y L, Ezer T et al. 2010. A three-dimensional surface wave-ocean circulation coupled model and its initial testing. *Ocean Dynamics*, **60**(5): 1339-1355, https://doi.org/10.1007/s10236-010-0326-y.

Qu T D. 2000. Upper-layer circulation in the South China Sea. *Journal of Physical Oceanography*, **30**(6): 1450-1460, https://doi.org/10.1175/1520-0485(2000)030<1450:ULCITS>2.0.CO;2.

Qu T D. 2003. Mixed layer heat balance in the western North Pacific. *Journal of Geophysical Research*: *Oceans*, **108**(C7): 35, https://doi.org/10.1029/2002JC001536.

Ren X J, Qian Y F. 2005. A coupled regional air-sea model, its performance and climate drift in simulation of the East Asian summer monsoon in 1998. *International Journal of Climatology*, **25**(5): 679-692, https://doi.org/10.1002/joc.1137.

Russo C S, Veitch J, Carr M et al. 2022. An intercomparison of global reanalysis products for Southern Africa's major oceanographic features. *Frontiers in Marine Science*, **9**: 837906, https://doi.org/10.3389/fmars.2022.837906.

Song W, Wang Y, Cui F J et al. 2019. Decadal variability of upper layer heat content and influencing factors in the South China Sea. *Oceanologia et Limnologia Sinica*, **50**(4): 752-758, https://doi.org/10.11693/hyhz20181100263. (in Chinese with English abstract)

Taguchi B, Schneider N, Nonaka M et al. 2017. Decadal variability of upper-ocean heat content associated with meridional shifts of western boundary current extensions in the North Pacific. *Journal of Climate*, **30**(16): 6247-6264, https://doi.org/10.1175/JCLI-D-16-0779.1.

Trott C B, Metzger E J, Yu Z T. 2023. Luzon strait mesoscale eddy characteristics in HYCOM reanalysis, simulation, and forecasts. *Journal of Oceanography*, **79**(4): 423-441, https://doi.org/10.1007/s10872-023-00686-5.

Uchiyama Y, Takaura N, Okada N et al. 2019. Residual circulations and associated water mass transport in the South China sea analyzed with a coupled HYCOM-ROMS downscaling ocean model. *AIP Conference Proceedings*, **2157**(1): 020029, https://doi.org/10.1063/1.5126564.

Vivier F, Kelly K A, Thompson L A. 2002. Heat budget in the Kuroshio extension region: 1993-99. *Journal of Physical Oceanography*, **32**(12): 3436-3454, https://doi.org/10.1175/1520-0485(2002)032<3436:HBITKE>2.0.CO;2.

Wang B. 2012. Observed and numerical study on the deep water circulation in the Luzon Strait and South China Sea. Ocean University of China, Qingdao, China. (in Chinese with English abstract)

Wang L, Huang K. 2016. Imprint of the ENSO on rainfall and latent heating variability over the Southern South China Sea from TRMM observations. *Journal of Ocean University of China*, **15**(2): 219-231, https://doi.org/10.1007/s11802-016-2766-6.

Wang X W, Liu Z Y, Peng S Q. 2017. Impact of tidal mixing on water mass transformation and circulation in the South China Sea. *Journal of Physical Oceanography*, **47**(2): 419-432, https://doi.org/10.1175/JPO-D-16-0171.1.

Yang H J, Liu Q Y. 1998. A summary on ocean circulation study of the South China Sea. *Advances in Earth Science*, **13**(4): 364-368, https://doi.org/10.3321/j.issn:1001-8166.1998.04.007. (in Chinese with English abstract)

Yu Z T, Metzger E J, Fan Y L. 2021. Generation mechanism of the counter-wind South China Sea Warm Current in winter. *Ocean Modelling*, **167**: 101875, https://doi.org/10.1016/j.ocemod.2021.101875.

Zhai F G, Wang Q Y, Wang F J et al. 2014. Variation of the North equatorial current, Mindanao current, and Kuroshio current in a high-resolution data assimilation during 2008-2012. *Advances in Atmospheric Sciences*, **31**(6): 1445-1459, https://doi.org/10.1007/s00376-014-3241-1.

Zhang P, Xu F, Tu S F et al. 2019. Spatial and temporal characteristics of the SSTA in the South China Sea from 1979 to 2017 and its correlation with the Walker circulation anomaly. *Journal of Marine Meteorology*, **39**(1): 15-25, https://doi.org/10.19513/j.cnki.issn2096-3599.2019.01.002. (in Chinese with English abstract)

Zheng F, Zhu J. 2015. Roles of initial ocean surface and subsurface states on successfully predicting 2006-2007 El Niño with an intermediate coupled model. *Ocean Science*, **11**(1): 187-194, https://doi.org/10.5194/os-11-187-2015.

Zhu Y H, Cao G J, Wang Y G et al. 2022. Variability of the deep South China Sea circulation derived from HYCOM reanalysis data. *Acta Oceanologica Sinica*, **41**(7): 54-64, https://doi.org/10.1007/s13131-021-1952-6.